Chem Biol Drug Des 2012; **80:** 862–875

Research Article

doi: 10.1111/cbdd.12006

Computational Studies of Novel Chymase Inhibitors Against Cardiovascular and Allergic Diseases: Mechanism and Inhibition

Mahreen Arooj[1], Sundarapandian Thangapandian[1], Shalini John[1], Swan Hwang[1], Jong K. Park[2] and Keun W. Lee[1,*]

[1]Division of Applied Life Science (BK21 Program), Systems and Synthetic Agrobiotech Center (SSAC), Plant Molecular Biology and Biotechnology Research Center (PMBBRC), Research Institute of Natural Science(RINS), Gyeongsang National University (GNU), 501 Jinju-daero, Gazha-dong, Jinju, 660-701 Korea
[2]Department of Chemistry Education, Research Institute of Natural Science (RINS), Educational Research Institute Teachers College, Gyeongsang National University, Jinju 660-701, Korea
**Corresponding author: Keun W. Lee, kwlee@gnu.ac.kr*

To provide a new idea for drug design, a computational investigation is performed on chymase and its novel 1,4-diazepane-2,5-diones inhibitors that explores the crucial molecular features contributing to binding specificity. Molecular docking studies of inhibitors within the active site of chymase were carried out to rationalize the inhibitory properties of these compounds and understand their inhibition mechanism. The density functional theory method was used to optimize molecular structures with the subsequent analysis of highest occupied molecular orbital, lowest unoccupied molecular orbital, and molecular electrostatic potential maps, which revealed that negative potentials near 1,4-diazepane-2,5-diones ring are essential for effective binding of inhibitors at active site of enzyme. The Bayesian model with receiver operating curve statistic of 0.82 also identified arylsulfonyl and aminocarbonyl as the molecular features favoring and not favoring inhibition of chymase, respectively. Moreover, genetic function approximation was applied to construct 3D quantitative structure–activity relationships models. Two models (genetic function approximation model 1 r^2 = 0.812 and genetic function approximation model 2 r^2 = 0.783) performed better in terms of correlation coefficients and cross-validation analysis. In general, this study is used as example to illustrate how combinational use of 2D/3D quantitative structure–activity relationships modeling techniques, molecular docking, frontier molecular orbital density fields (highest occupied molecular orbital and lowest unoccupied molecular orbital), and molecular electrostatic potential analysis may be useful to gain an insight into the binding mechanism between enzyme and its inhibitors.

Key words: Bayesian categorization, chymase, genetic function approximation, molecular docking, quantitative structure–activity relationship

Abbreviations: ACE, angiotensin-converting enzyme; Ang-I, angiotensin-I; Ang-II, angiotensin-II; DFT, density functional theory; DS, discovery studio; GFA, genetic function approximation; GOLD, genetic optimization for ligand docking; His, histidine; HOMO, highest occupied molecular orbital; LUMO, lowest unoccupied molecular orbital; MESP, molecular electrostatic potential; PDB, protein data bank; Phe, phenylalanine; RMSD, root mean square deviation; SAR, structure–activity relationship; TGF-β, transforming growth factor-β; Trp, tryptophan; Tyr, tyrosine.

Received 3 April 2012, revised 30 May 2012 and accepted for publication 4 July 2012

Assessing ligand orientation and the strength of ligand…receptor interactions is befitted as an essential component of modern drug discovery and prolific approaches, and programs are available to model ligand at the respective active site. In the course of investigating ligand binding, acquiring the best conformation and orientation of the ligand in the binding pocket along with the accurate estimates (or score) of binding affinities (generally referred to as the 'docking problem') are normally distinguished as the major tasks (1). As interactions between molecules are the consequence of their stereoelectronic properties that govern strength of bonds, strength of non-bonded interactions, and molecular reactivity, therefore, analysis of molecular electronic features such as electron density, frontier molecular orbital density fields such as lowest unoccupied molecular orbital (LUMO), highest occupied molecular orbital (HOMO), and molecular electrostatic map (MEP) is quite significant to elucidate the orientation and the strength of ligand–receptor interactions (2,3). Exploration of electronic features also plays an imperative role in divulging the relationship between biological activity and electronic molecular properties of inhibitors (4). For instance, the HOMO density field was useful in a study of angiotensin-converting enzyme (ACE) inhibitors, and LUMO density field was found to be important for explaining the TA100 mutagenicity (5,6). The mapping of the electrostatic potential is an established technique for investigation of biologically active compounds and constitutes a vital element of a 3D quantitative structure–activity relationships (QSAR). The QSAR as one of the most important areas in computational drug design gives information that is useful for drug discovery and medicinal chemistry. Moreover, QSAR

study is a helpful approach to quantitatively understand the relationships between molecular structures of inhibitors and their biological activities (7,8). Therefore, a computational strategy combining 2D/3D QSAR modeling techniques along with molecular docking and quantum chemical methodologies is a good endeavor to gain an insight into the interactions between active site of the enzyme and ligands and to explain the associations involving molecular biological activities of ligands.

The renin–angiotensin system or the renin–angiotensin–aldosterone system is a hormone system that regulates blood pressure and water (fluid) balance. Angiotensin-II (Ang-II) is the major effector hormone of this system. The octapeptide hormone, Ang-II, targets human heart and plays an important role in vascular proliferation, hypertension, and atherosclerosis (8). Conversion of angiotensin-I (Ang-I) to Ang-II is catalyzed by well-known enzyme (ACE), which is a metalloproteinase with dipeptidyl carboxypeptidase activity. However, chymase (EC 3.4.21.39), which is a chymotrypsin-like enzyme expressed in the secretory granule of mast cells, also catalyzes the production of Ang-II in vascular tissues even when ACE is blocked (Figure 1). Chymase converts Ang-I to Ang-II with greater efficiency and selectivity than ACE (9). The rate of this conversion by chymase is approximately fourfold higher than ACE. To generate Ang-II, human chymase cleaves the Ang-I at Phe8-His9 peptide bond. Chymase shows enzymatic activity immediately after its release into the interstitial tissues at pH 7.4 following various stimuli in tissues. As chymase has no enzymatic activity in normal tissues, chymase inhibitors have the potential to be safe/non-toxic, because specific chymase inhibitors may not have effects on any other targets in normal tissues (10). Chymase also converts precursors of transforming growth factor-β (TGF-β) and matrix metalloproteinase (MMP)-9 to their active forms, thus contributing to vascular response to injury (Figure 1). Both TGF-β and MMP-9 are involved in tissue inflammation and fibrosis, resulting in organ damage (11). Previous studies have demonstrated the involvement of chymase in the escalation of dermatitis and chronic inflammation pursuing cardiac and pulmonary fibrosis (12). Therefore, inhibition of chymase is likely to facilitate the treatment of cardiovascular diseases, allergic inflammation, and fibrotic disorders. Chymase inhibition may also be useful for preventing the progression of type 2 diabetes, along with the prevention of diabetic retinopathy (13). Moreover, role of chymase in inflammation has prompted its restorative value in diseases such as chronic obstructive pulmonary disease and asthma (14).

Human chymase is folded into 2-six-stranded b-barrels, which are connected by three trans-domain segments as illustrated in Figure S1. Additional regular secondary structure elements are a helical loop between residues 56 and 59, an irregular 'intermediate' helix involving residues 165–173, and a long C-terminal helix stretching from Tyr234 to Asn245. In human chymase, the inhibitor binding region is defined by residues Lys40, His57, Tyr94, Asn95, Thr96, Leu99, Asp102, Ala190, Phe191, Lys192, Gly193, Ser195, Val213, Ser214, Tyr215, Gly216, and Arg217 (Figure S1). The region is mostly polar because of main chain carbonyls that are arranged along the surface of the region. In general, chymase inhibitors readily decompose in plasma; thus, the stability of the chymase inhibitors in human plasma has always been a matter of great concern. For a drug candidate, it is essential to enhance the stability of the active compound in human plasma. Consequently, there is always a dire need to search for more stable inhibitors with high activity against human chymase. Several chymase inhibitors such as sulfonyl fluoride derivatives(15), Boc-Val-Pro-Phe-CO_2Me(16), Z-Ile-Glu-Pro-Phe-CO_2Me (Z is benzyloxycarbonyl), (F)-Phe-COGlu-Asp-ArgOMe (17), *N*-(2-Naphthyl) carboxamido derivatives (18), *N*-[2,2-dimethyl-3-(*N*-(4-cyanobenzoyl)amino)nonanoyl]-L-phenylalanine ethyl ester (19), 3-benzylazetidine-2-one derivatives (20), 1,3-diazetidine-2,4-dione derivatives (21), methyllinderone derivatives (22), chloromethyl ketone derivatives (23), 1-oxacephem derivatives (24), and 3-(phenylsulfonyl)-1-phenylimidazolidine-2,4-dione derivatives (25) have been reported previously. Various QSAR studies for chymase inhibitors have been performed. The QSAR analysis of anhydride-type chymase inhibitors showed that aromatic substituents played an important role in determining the inhibitory potency of the compounds (26). Moreover, Hayashi *et al.* (23) showed that introduction of various substituents in chloromethyl ketone derivatives resulted in variation in their activity against human chymase.

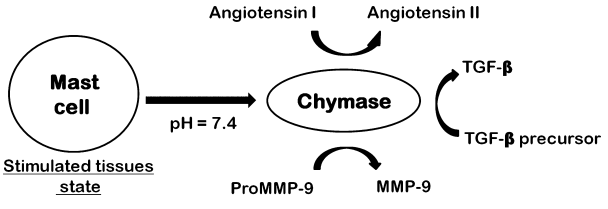

Figure 1: Chymase-dependent conversion of angiotensin I to angiotensin II and precursors of transforming growth factor (TGF)-β and matrix metalloproteinase (MMP)-9 to their active forms.

The present group of authors have developed 1,4-diazepane-2,5-diones derivatives as novel classes of chymase inhibitors that are potent, stable, and orally active with high selectivity and efficacy (27,28). Although this series of compounds have been developed using classical and intuitive medicinal chemistry approaches, little information is available about the structure–activity relationship (SAR) of these compounds. As the number of active compounds in a series increases, formulation of useful SAR data becomes increasingly difficult (29). Moreover, the molecular mechanism by which these compounds act still remains unclear. The main goal of the study presented below is to develop QSAR models and to explore the key molecular features influencing the protein–ligand binding and interaction for 1,4-diazepane-2,5-diones derivatives using molecular docking, advanced quantum chemistry techniques, and 2D/3D QSAR molecular modeling approaches. In first phase of current research exertion, the docking method was employed to generate models of the 3D bioactive conformations of inhibitors that served as the initial input structures for further geometric optimization with the density functional theory (DFT). Based on quantum chemical calculations, maps for frontier molecular orbital density fields (HOMO and LUMO) and MEP were calculated and produced. These precise quantum chemical descriptors along with docking poses were used to analyze electronic structure of the ligands and the binding interactions between ligands and the key active site residues of chymase. In next phase, 2D and 3D QSAR models were developed to explore the dependence of inhibitory activities of 1,4-diazepane-2,5-diones derivatives upon various physiochemical properties using Bayesian

modeling and genetic function approximation (GFA) modeling approaches. For the identification of the regions in inhibitors that were likely important for chymase inhibition as well as substructures that were associated with less-active inhibitors, a Bayesian model with 2D molecular descriptors was developed. Furthermore, GFA models were constructed using molecular docking parameters (external van der Waals, internal van der Waals, and external hydrogen-bonding interactions) along with DFT-based parameters and other 2D and 3D physiochemical properties of inhibitors. The results of this study are expected to be useful for understanding the molecular mechanism by which these compounds act and can be further utilized to guide the design of compounds with better antichymase activity by rational modification.

Methods and Materials

Data set

To a great extent, the bioactivity of a ligand against a receptor relies on its binding tropism, which primarily depends on the structurally steric orientation and the electrostatic property. It is customary that small structural difference may give rise to great biological diversity. Therefore, based on structural diversity and wide biological activity range, chymase inhibitors, 15 from 6-benzyl substituted 4-aminocarbonyl-1,4-diazepane-2,5-diones, and 20 inhibitors from 6-substituted 4-arylsulfonyl-1,4-diazepane-2,5-diones were selected. Thus, data set employed in this study consists of 35 compounds, and 2D chemical structures of these compounds are depicted in Figure 2.

Molecular docking

Docking plays a significant role in the prediction of the binding orientation, affinity, and activity of small molecule drug candidates to their protein targets with known 3D structures. Hence docking serves as an important tool in the rational computer-assisted drug design (30,31). The 3D ligand structures were downloaded from public database [i.e., the BindingDB (http://www.bindingdb.org) (32). For all the compounds in our data set, energy minimization process was performed with CHARMm Forcefield option as available in Accelrys Discovery Studio v2.5 (DS), Accelrys, San Diego, USA using Smart Minimizer protocol. This protocol performs 1000 steps of Steepest Descent with a RMS gradient tolerance of 3, followed by conjugate gradient minimization. Compounds with minimum energy served as the input structures for docking using GOLD 5.0.1 (Genetic Optimization for Ligand Docking) program (33,34). The GOLD 5.0.1 from Cambridge Crystallographic Data center, UK, uses a genetic algorithm for docking ligands into protein binding sites to explore the full range of ligand conformational flexibility with partial flexibility of protein (35). Molecular docking was performed to generate the models of bioactive binding poses of inhibitors in the active site of enzyme. Protein co-ordinates from the crystal structure of chymase co-crystallized with β-ketophosphonate (protein data bank (PDB) ID: 1T31), determined at a resolution of 1.9 Å, were used to define the active site (14). All the water molecules present in the protein were removed, and hydrogen atoms were added using CHRAMM22 force field as available in DS. The active site was defined with a 10-Å radius around the geometric center of the ligand present in the crystal structure. At the end of the computation, the 10 top-scoring conformations of every ligand were saved. Early termination option was applied to pass over the genetic optimization calculation when any five conformations of a particular compound were envisaged within an RMS deviation value of 1.5 Å. The GOLD fitness score is calculated from the contributions of hydrogen bond and van der Waals interactions between the protein and ligand, intramolecular hydrogen bonds, and strains of the ligand. The protein–ligand interactions were examined by DS.

Density functional theory calculations

The best-scoring poses of each ligand generated with docking were used as input for DFT calculations. All DFT computations were carried out using the Gaussian 03 suite of programs. Hybrid Becke's three-parameter exchange potential and the Lee–Yang–Parr correlation functional (B3LYP) method were employed to optimize the geometries of chymase inhibitors at 6-31G* level within the self-consistent fields (36).

Molecular electrostatic potential calculations

Molecular electrostatic potential (MEP) is widely used in characterizing molecules, especially for biomolecules, and takes special effect in the biomolecular recognition and in the prediction of the functional sites (37,38). The electrostatic potential, V(r), that the electrons and nuclei of a molecule create at each point r in the surrounding space is given by

$$V(r) = \sum \frac{Z_A}{|R_A - r|} \int \frac{\rho(r')}{|r' - r|} dr'$$

where Z_A is charge on nucleus A, located at R_A, and ρ (r) is the electronic density function of the molecule. The potential, V(r), is a real physical property determined computationally. The regions where V(r) is negative, the contribution of the electrons predominates, and for the positive valued regions, depletion of the charge is observed. For the MEP calculations, we define the surface in terms of a molecular property, namely the total electronic density function. This surface easily provides the set of points needed, and a color mapping of the electrostatic potential at this surface provides a highly informative visualization in chemical studies. In particular, this color-coded depiction of the molecular anatomy provides more information on the reactive potential of a molecule. In this work, the electrostatic properties are calculated using DFT at the B3LYP/6-31G* level. The formatted checkpoint files of the compounds generated by the geometric optimization computation were used as input for CUBEGEN program interfaced with Gaussian 03 program to compute the MEP. The MEP isopotential surfaces were produced and superimposed onto the total electron density surface (0.0004 e/au^3). The electrostatic potential of the whole molecule is finally obtained by superimposing the electrostatic potentials upon the total electron density surface of the compound.

2D and 3D QSAR models building

Quantitative structure–activity relationship (QSAR) analysis refers to methods for developing mathematical relationships between biological activity and computed (or measured) properties. For this

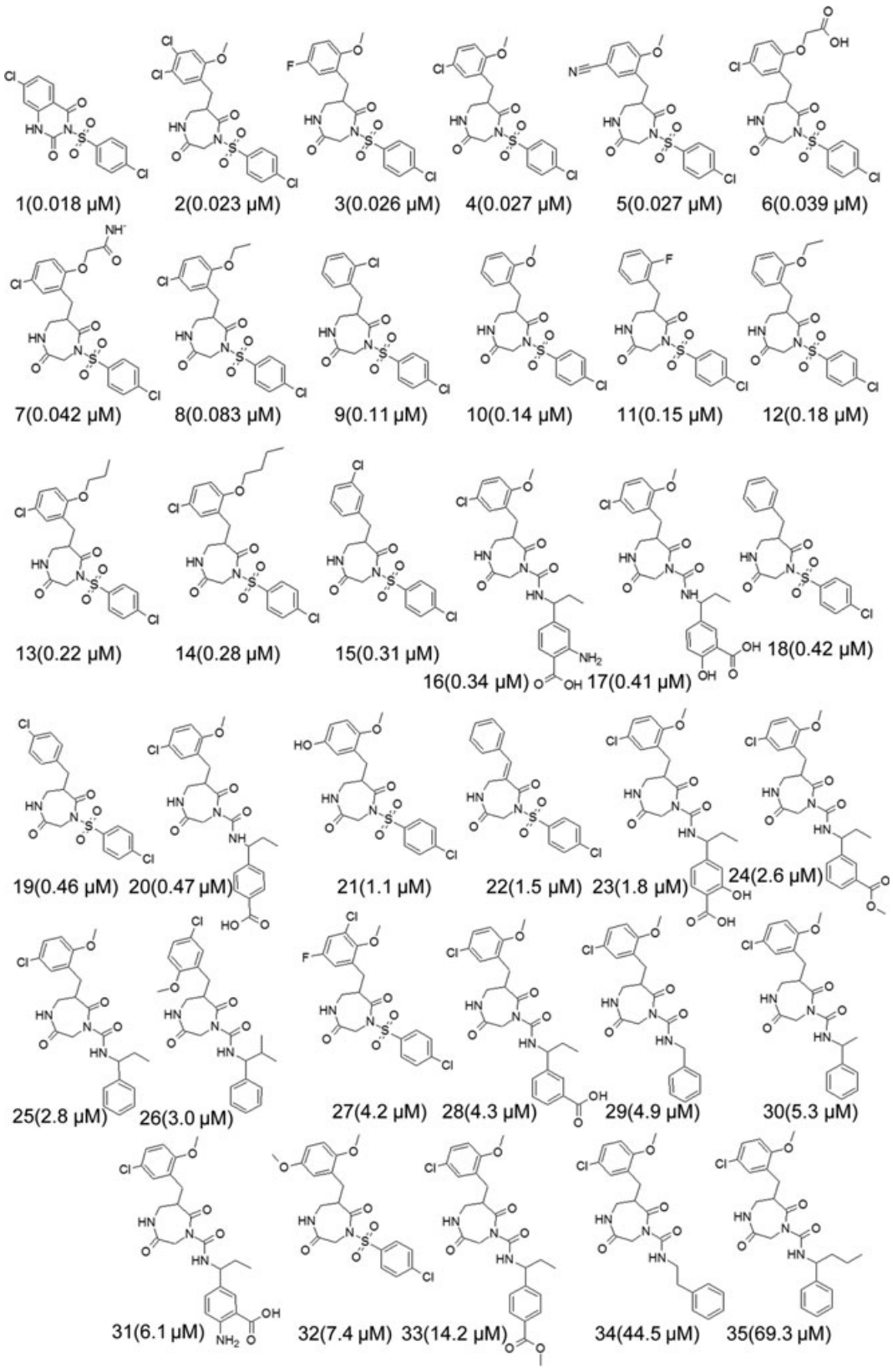

Figure 2: Two-dimensional chemical structures of 1,4-diazepane-2,5-diones with their anti-chymase bioactivities used in the present study.

research exertion, QSAR models were generated by applying following two QSAR approaches.

Bayesian model development

A Bayesian model incorporated with 2D descriptors (molecular function class fingerprints of maximum diameter 6 (FCFP_6), AlogP, molecular weight, number of hydrogen bond acceptors, number of hydrogen bond donors, number of rotatable bonds, number of rings, number of aromatic rings, and molecular fractional polar surface area) was generated using DS. For Bayesian model generation, a training set of 15 compounds labeled as **1,2,4,6,12,14, 15,19,22,24,25,27,31,32,34** assimilating biological and chemical diversity was developed. The 'Create Bayesian Model' protocol was used for model generation. A leave-one-out (LOO) cross-validation receiver operating curve (ROC) was obtained for the validation of the generated Bayesian model. Generation of model lead to the identification of good and bad molecular features favoring inhibition and not favoring inhibition, respectively, of training set compounds.

Genetic function approximation models development

Genetic function approximation was employed to search for the best possible QSAR regression equation capable of correlating the variations in biological activities of the compounds with variations in the generated descriptors (39). Genetic function approximation is performed as follows: (i) An initial population of equations is generated by random choice of descriptors. The 'fitness' of each initial equation for calculating an activity index over the training data set is scored by using Friedman's lack-of-fit (LOF) measure:

$$\mathrm{LOF} = \mathrm{LSE}/\{1 - (c + d^{*}p)/m\}^{2}$$

where LSE is the least-squares error (calculated from the difference between actual and calculated values for the activity index over data set), c is the number of basis functions in the model, d is a smoothing parameter that controls the number of terms in the model equation (a larger value of d leads to fewer terms), p is the number of features contained in all terms of the model, and m is the number of samples (compounds) in the training set. The LOF measure penalizes appropriately for the addition of terms to the equation (and consequent loss of degrees of freedom) in such a way as to resist overfitting. (ii) pairs from the population of equations are chosen at random and 'crossovers' are performed and progeny equations are generated; (iii) The fitness of the progeny equation is assessed by calculating the LOF measure. (vi) If the fitness of new progeny equation is better, then it is preserved. The models with proper balance of all statistical terms are used to explain variance in the biological activity. A distinctive feature of GFA is that it produces a population of models (e.g., 100), instead of generating a single model, as do most other statistical methods. The range of variations in this population gives added information on the quality of fit and importance of the descriptors. Because of additional information about the models, this algorithm produces superior models in comparison with traditional stepwise or similar techniques (40).

To obtain GFA models, pIC50 of the compounds was employed as dependent variable. Various physiochemical properties of the compounds were designated as descriptors utilized for QSAR construction. The ligand's physiochemical properties incorporate 2D (AlogP, Surface Area and volume descriptors such as Molecular_Fractional-PolarSASA, Molecular_PolarSurfaceArea, and Molecular_PolarSASA, etc., topological descriptors such as BIC,CHI_0,CHI_3_P, CIC, IAC_-Mean, IAC_Total, IC and E_DIST_equ, etc.) and 3D (Dipole, Jurs descriptors, shadowindices andMolecular_Volume, etc.) parameters. All the definition of the descriptors can be seen in the Help Topics of DS software, and they were computed by QSAR protocol of DS (23). Moreover, docking parameters that constitute external H-bonding, external van der Waals interaction, and internal van der Waals interaction were also used along with quantum mechanical descriptors (HOMO and LUMO) as independent variables for the formation of GFA models. The selection of the derivatives in the training set was made according to the structure and the scale of the biological action, so that representatives of a wide range of structures (in terms of the different substituents, atoms, and action) were included. According to Golbraikh and Tropsha, this approach is correct as representative points of the test set must be close to those of training set and vice versa (41). As the predictability of a QSAR model is best judged by the external validation using a test set compounds, the data set was divided into training and test sets. Training set included compounds labeled as **1,2,4,6,12,14,15, 19,22,24,25,27,31,32**, and **34**. We adopted multiple validation strategies like LOO cross-validation and external validation. The predictive ability of the models was estimated from the prediction of the chymase inhibitory activity of a test set of 12 compounds including **5,7,8,9,10,11,13,18,20,26,29,35**.

Results and Discussion

Molecular docking

The docking procedure proposes energetically favorable conformations and orientations of ligands in the binding pocket of a protein and predicts key interactions. In this study, docking analysis is performed to predict binding conformations and to define which residues and which types of interactions are involved in the binding of the ligands.

Validation of ligand binding mode

The docking investigation has been performed with GOLD 5.0.1. Molecular docking program GOLD has been validated for a large number of protein complexes and performed better for most of the proteins. However, it also did poor for many protein–ligand complexes. Thus, a validation process is executed to verify whether or not GOLD can perform better for chymase by docking an inhibitor molecule for which the binding conformation is identified crystallographically. Crystal structure with the PDB code 1T31 bound with an inhibitor molecule was selected as receptor, and the active site was defined with a 10-Å radius around the ligand present in the crystal structure. The top conformation predicted by GOLD program was very close to the crystal structure–bound conformation. The root mean square deviation (RMSD) between the docked pose and its bound conformation in the crystal structure is 0.76 Å, indicating

that GOLD was able to reproduce correct pose (Figure 3). Docking experiments were further performed with crystal structures of chymase including 3N7O and 3SON. Comparison of the docked pose and the crystallographic mode was performed for both structures. The RMSD values between the docked pose and its bound conformation for 3N7O and 3SON are 0.53 and 0.81 Å, respectively, thus indicating that GOLD performed well for chymase. The top and side views of the docked poses of the ligands and their bound conformations in the crystal structures are illustrated in Figure S2. After this validation, all of the 35 inhibitors of chymase in the data set were docked into the X-ray crystallographic structure of human chymase coded as 1T31 in PDB, and the 10 top-scoring conformations of every inhibitor are saved. All of the inhibitors in the study were docked using the same method, and their interactions were analyzed. Only the interactions of selected most-, mid-, and least-active inhibitors are discussed in detail. The orientation and important interactions of the most-active inhibitors, **2**, **4**, and **16**, with the key residues within the active site of chymase are shown in Figure 4. In compound **2**, various hydrogen bonds between the carbonyl oxygen of the 7-membered 1,4-diazepane-2,5-diones ring system and Gly193 and Ser195 residues of the active site are formed. Previous studies of chymase have also divulged the importance of Gly193 and Ser195 as key amino acids in active site region of the enzyme (14,18). Benzenesulfonyl chloride group of compound **2** is fully enclosed by the residues of the S1 pocket and capped with the side chain of Phe191. This placement leads to π–σ interaction between the σ system of Phe191 and the benzene ring of benzenesulfonyl chloride group in compound **2**. The binding is further stabilized by the π–π interaction between His57 and benzene ring of the 1-chloro-4-methoxybenzene group in an oscillating manner. Along with diverse hydrogen-bonding contacts, presence of π–π and π–σ interactions in compound **2** appears to have a significant role in its activity. Docking analysis of compound **4** revealed that benzenesulfonyl chloride group was placed in oxyanion hole formed by Ser195 and Gly193 amino acids. The oxygen atoms of sulfonyl formed hydrogen bond interactions with hydroxy of Ser195 and amide NH of Gly193, while carbonyl oxygen of 7-membered ring in compound **4** showed hydrogen bond contacts with amino acids of the hydrophobic S1` pocket of enzyme. Such kinds of interactions of inhibitors with the active site were also revealed in a 3D QSAR model for chymase (42). Compound **16** showed important interactions between the Ser195 and Lys192 residues of the active site through 1-chloro-4-methoxybenzene group and carbonyl oxygen of the 1,4-diazepane-2,5-diones ring. Substitution of less electron–withdrawing aminocarbonyl group on the 4-position of the 1,4-diazepane-2,5-dione scaffold lead to the formation of mid-active compounds **25** and **27**. The binding conformation of mid-active compound **25** was rather different from the binding conformations of other most-active compounds. It exhibited hydrogen bond interactions between halogen-substituted benzene group and Ser195. Substitution of halogen at C5 was mainly interpreted as space filler. However, the role of halogen at C5 can be seen as the stabilizing factor in the molecular recognition. The halogen here is not just space filler but is involved in polar interactions. In addition to the conventional or strong hydrogen bonds, electrostatic $\pi\ldots$ + interactions between benzene ring of compound **25** and highly basic Arg143 amino acid, acting in concert, made a contribution to the binding specificity of the ligand in the active site. Inspection of binding conformation of mid-active compound **27** exposed the presence of various hydrogen bond interactions with the key active site residues. Carbonyl oxygen of 7-membered ring exhibited hydrogen bonding with amide of Gly193. Moreover, compound **27** also made close contacts that lead to the important ligand–enzyme interaction such as hydrogen-bonding interactions with Ser195 and hydrophobic interactions with His57 amino acid in the active site of the enzyme. The orientations of the least-active compounds, **34** and **35**, are almost similar to that of most-active and mid-active compounds. However, no good coordination was achieved for the case of the least-active compounds; only two hydrogen bonds are present when compared with most-active compounds, as shown in Figure 4. In addition, the absence of favorable electrostatic interactions is also probably part of the reason for their low activity.

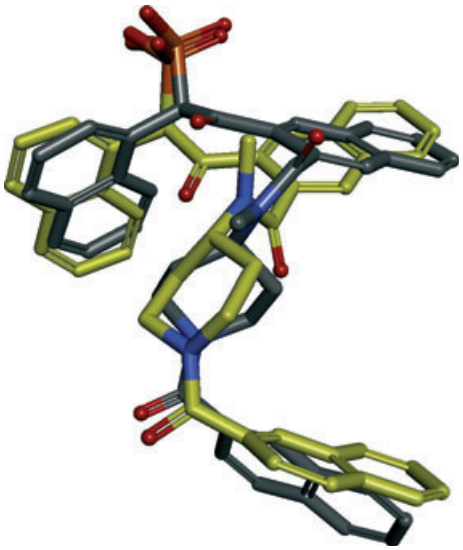

Figure 3: Overlay of the docked pose (grey) of inhibitor with its crystal structure conformation (yellow). Hydrogen atoms are removed for clarity.

Density functional theory calculations

Electronic structure

This part of Results section contains the electronic structure description for investigated compounds. The outline of this part is as follows: first, the electron density and electrostatic potential distribution are analyzed using isosurface maps. Next, plots of quantum chemical descriptors such as LUMO and HOMO are analyzed to show the bonding and atomic charges distribution.

Molecular electrostatic potential profiles

Molecular electrostatic potential mapping is an established technique in the investigation of the molecular structure with its physiochemical property relationships. The MEP is very important for bioactive compounds, because it plays a key role in the initial steps of ligand–receptor interactions. The MEP varies in its magnitude within the space occupied by a molecule. This is seen from the

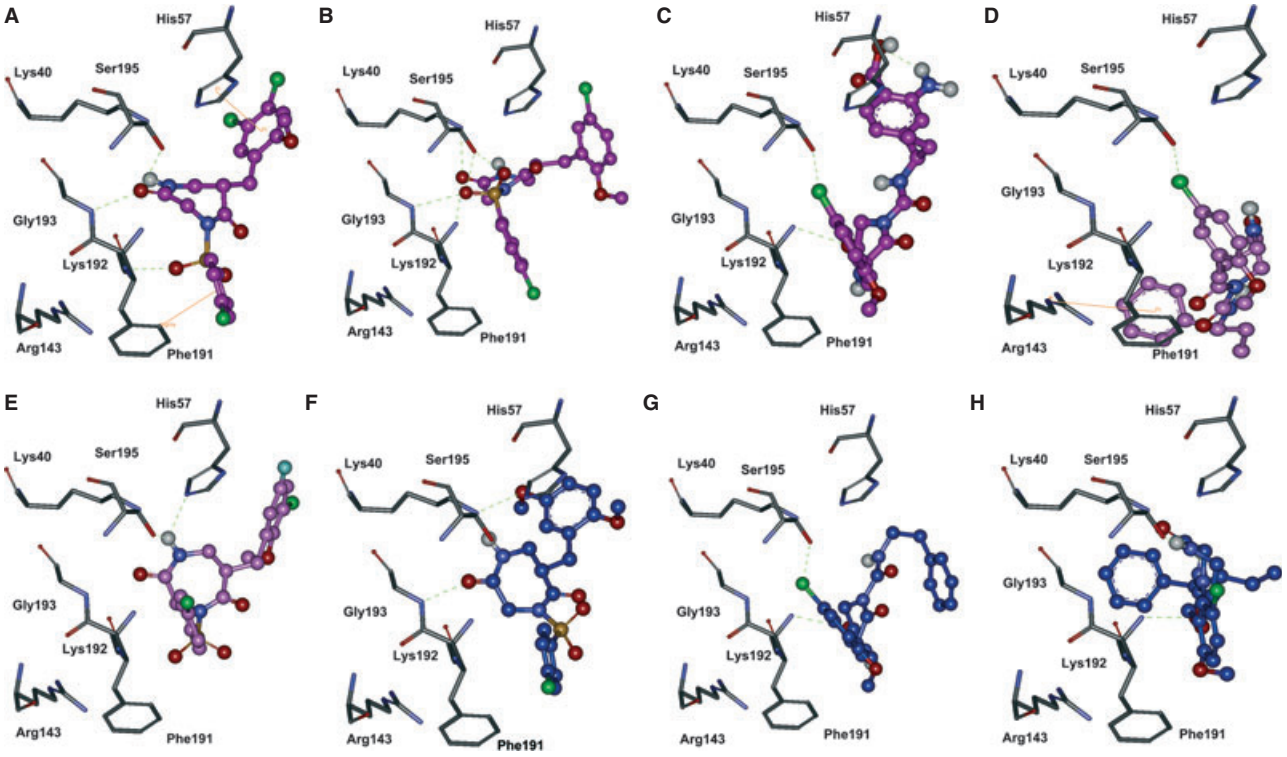

Figure 4: Molecular docking results. The binding modes and molecular interactions of most-active **2** (A), **4** (B), **16** (C), mid-active **25** (D), **27** (E), and least-active compounds **32** (F), **34** (G), **35** (H). The key active site residues and inhibitors are shown in stick and ball-stick forms, respectively. The hydrogen bonds between protein and inhibitors are shown in green dashed lines. Hydrogen atoms are removed for clarity.

results of computation of the electrostatic potential on a defined set of points surrounding the molecule. We can, thus, compute electrostatic potential on the three-dimensional molecular surface. The electron density is represented by the nature and intensity of color. The red color corresponds to high accumulation of charge, that is, the negatively charged region, and the blue color corresponds to charge depletion, that is, the positively charged region. The green color corresponds to the neutral regions. The 3D isosurface maps of MEP for all compounds were interpolated on the electron density surfaces of constant electron charge density (0.0004 e/au^3.).

The 3D MEP plots of the most-active and mid-active compounds, **2**, **4**, **16** and **25**, **27**, respectively, along with least-active compounds, **32, 34**, and **35**, are illustrated in Figure 5. The results show that all most-active compounds share specific electronic properties and are different from least-active/mid-active compounds. The MEP plotted onto constant electron density surface for all most-active compounds showed the most electropositive potential region (blue color) near the protons of C3 and C4 of the 1-chloro-4-methoxybenzene and protons of C6 and C7 of the 1,4-diazepane-2,5-diones ring system. One more prominent localized positive-charged region was seen over the C2 and C3 of benzenesulfonyl chloride moiety. Thus, overall electropositive potential of the most-active compounds formed an inverted V-shaped region, while electronegative potential was spread over the carbonyl oxygen of the 7-membered ring system and oxygen atoms of benzenesulfonyl chloride group. In addition, carbon atoms attached with halogen atoms predominated the green region in the MEP surfaces of the most-active compounds. The MEP isosurface of compound **2** is superimposed inside the active site of chymase (Figure 6). On the whole, appearance of both most electronegative and electropositive regions illustrates that these regions can act as electron donors or acceptors to the active site of the chymase, thus making these compounds very reactive. Docking results of these compounds also indicated the involvement of these areas in the important interactions with the key active site residues such as Ser195, Gly193, His57, and Phe191 of the enzymes. The analysis of MEP maps of the mid-active/least-active compounds showed the absence of inverted V-shaped electropositive potential region in their maps. Moreover, a gradual depletion of both red and blue areas and an increase in green-colored region in the MEP maps of mid-active/least-active compounds were also observed. However, MEP of mid-active compounds exhibited more positive and negative potential regions than least-active compounds. The positive potential because of protons of C3 and C4 of the 1-chloro-4-methoxybenzene was also missing in least-active compounds. It is suggested that attack on the lactam carbonyl at the 5-position of 6-substituted-4-arylsulfonyl-1,4-diazepane-2,5-diones derivatives by the activated hydroxyl group of the key amino acid Ser195 of the binding site may transform chymase into an inactivated form, the acylated enzyme (28). The reactivity of the lactam carbonyl at the 5-position is activated by the electron-withdrawing group arylsulfonyl substituted at the 4-position. Most probably, this reactivity plays an important role in the acylation process of the serine residue of the active site, as well as instability in aqueous media. In this sense, the critical role played by the 4-

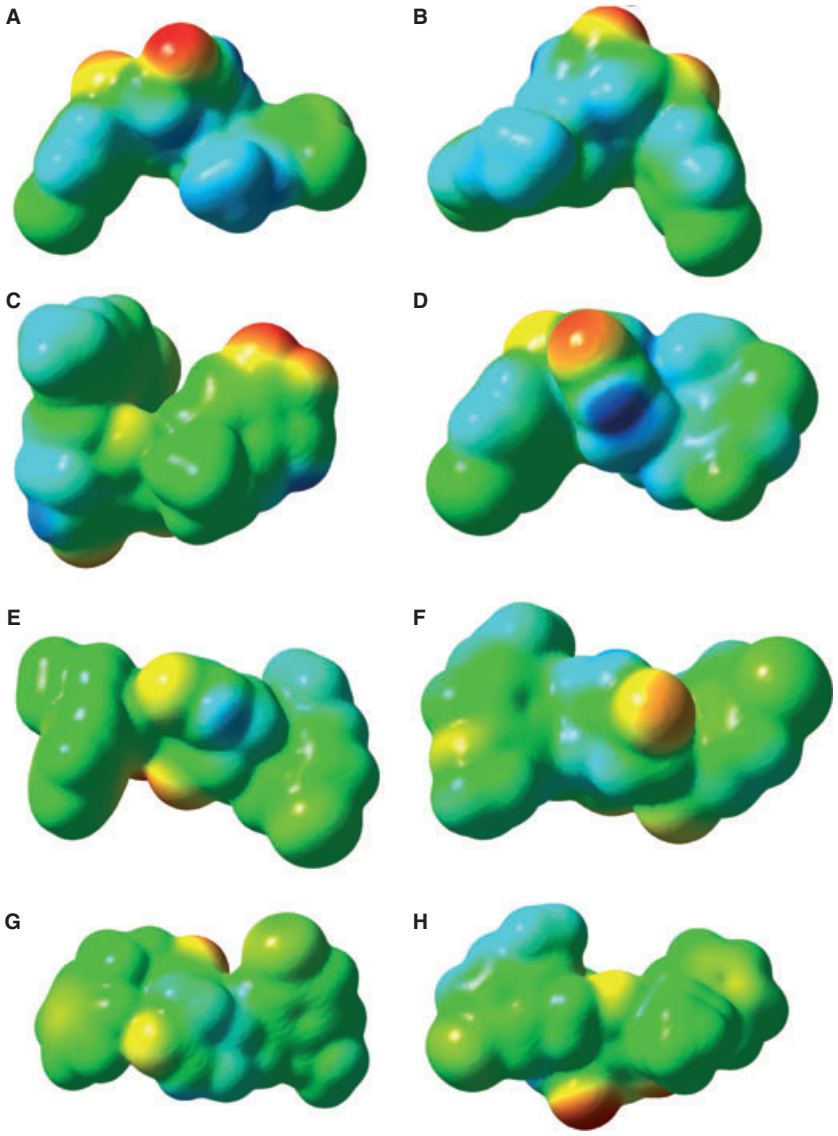

Figure 5: Molecular electrostatic potential (MEP) maps of most-active **2** (A), **4** (B), **16** (C), mid-active **25** (D), **27** (E), and least-active compounds **32** (F), **34** (G), **35** (H). The red and the blue color represent the electronegative and electropositive potentials, respectively, whereas the green represents a potential halfway between the two extremes.

substituent for activity is remarkable. To reduce the reactivity of the lactam carbonyl in 1,4-diazepane-2,5-diones ring system, the arylsulfonyl group was replaced with the less electron–withdrawing aminocarbonyl at the 4-position. Most of the mid-active and least-active compounds belong to the 1,4-diazepane-2,5-diones scaffold with aminocarbonyl group. This substitution in mid/least-active compounds instigated to the disappearance of both electropositive and electronegative potential regions that were present on carbon and both oxygen atoms of benzenesulfonyl chloride moiety, respectively. The strong electrostatic interaction of the negative potential with key residues Gly193 and Ser195, namely the formation of the hydrogen bond, enhanced the inhibition effect substantially, as this region was involved in important ligand-binding interaction with the key active site residues; thus, substitution of less electron–withdrawing aminocarbonyl lead to accumulation of less electronegative potentials that subsequently affected activity of the compounds. Hence, it is apparent from these results that the negative potentials near 1,4-diazepane-2,5-diones ring are crucial for activity. A previous study also showed that presence of hydrogen bond acceptor sites for a chymase inhibitor was important for its effective binding with the key residues of the active site (42). Thus, presence of such negative potentials in a chymase inhibitor is the structural requirement, and electrostatic potential features of the current study are also consistent with it.

Lowest unoccupied and highest occupied molecular orbitals

Highest occupied molecular orbital and LUMO sites are plotted onto the molecular surface of most-active and mid-active compounds, **2**, **4**, and **25**, **27**, respectively, along with least-active compounds, **34** and **35**, as shown in Figure 7. According to Frontier Orbital Theory, the shapes and symmetries of the HOMO and LUMO are crucial in predicting the reactivity of a species and the stereochemical and regiochemical outcome of a chemical reaction. Thus, the results obtained from these quantum chemical descriptors led us to characterize the reactive sites and substituent influence on electronic structure of the compounds. Analysis of HOMO maps of compounds

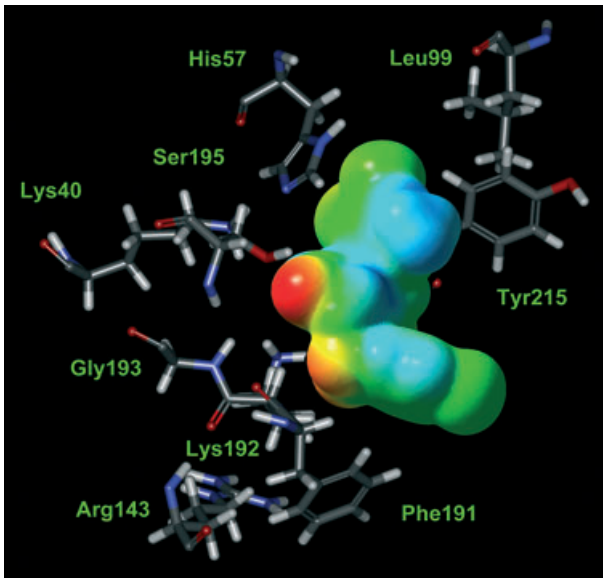

Figure 6: The superimposition of molecular electrostatic potential (MEP) map of compound **2** upon the active site of chymase.

illustrate that HOMO molecular orbitals are located on the 1-chloro-4-methoxybenzene indicating the existence of a possible reactive sites; therefore, electrophilic attacks from the residues of the active site of enzyme might take place on these sites. Docking results of these compounds also revealed the involvement of 1-chloro-4-methoxybenzene group in important hydrogen bond interactions with the key residues of the active site, while LUMO maps are plotted on the electron-withdrawing benzenesulfonyl chloride and 2-aminobenzoic acid groups of the compounds. However, in case of compounds **25** and **35**, LUMO plot was scattered over a part of 1,4-diazepane-2,5-diones ring along with benzene ring of the 1-chloro-4-methoxybenzene group. These results are quite consistent with the docking analysis and MEP profiles of the compounds that illustrate the participation of these moieties in the key ligand–receptor interactions.

Development of 2D and 3D QSAR models

Bayesian model

The training set of 15 compounds was applied to develop a Bayesian model with molecular function class fingerprints of maximum diameter 6 (FCFP_6) and eight interpretable descriptors. Of 15 compounds, eight most-active compounds were selected as 'active' with a value '1' and rest of the compounds were given a value '0' to allocate them 'not active'. Each compound was left out one at a time, and a model was built using the results of the compounds and that model was used to predict the left-out compound. Once all the compounds had predictions, a receiver operator curve (ROC) plot was generated, and the area under the curve was calculated. The model had a LOO cross-validation ROC statistic of 0.82 and enrichments that suggested that chymase most-active inhibitors were well separated from less-active inhibitors (Figure 8). The best split value that demarcated most-active inhibitors from less-active inhibitors was calculated by minimizing the number of compounds that were incorrectly predicted as either inhibitors or non-inhibitors,

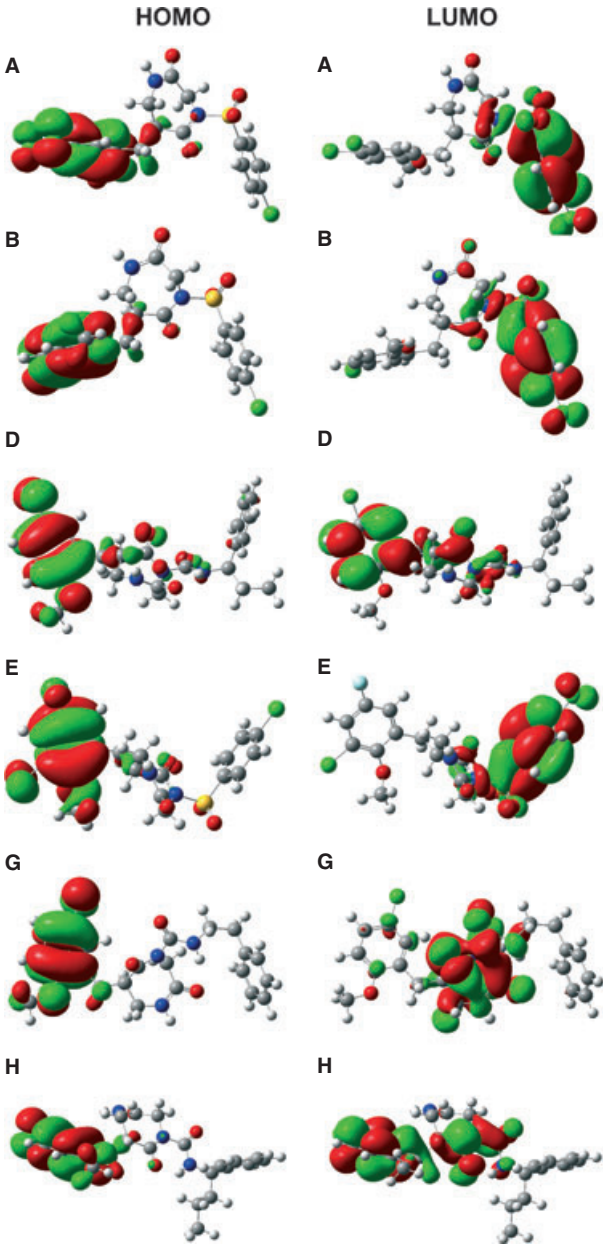

Figure 7: Plots of highest occupied molecular orbital (HOMO) and lowest unoccupied molecular orbital (LUMO) of most-active **2** (A), **4** (B), mid-active **25** (D), **27** (E), and least-active compounds **34** (G), **35** (H).

using the cross-validated score for each compound. Using that split, a contingency table is constructed (Table 1), containing the number of true positives (TP), false negatives (FN), false positives (FP), and true negatives (TN). This Bayesian model with 2D fingerprints also represents a classification approach to building models that can be used for rapid screening of compound libraries. From the molecular fingerprints, descriptors identified regions in the training set molecules that were likely important for chymase inhibition as well as substructures that were associated with less-active inhibitors. Top five fingerprints of both categories are demonstrated in Figure 9.

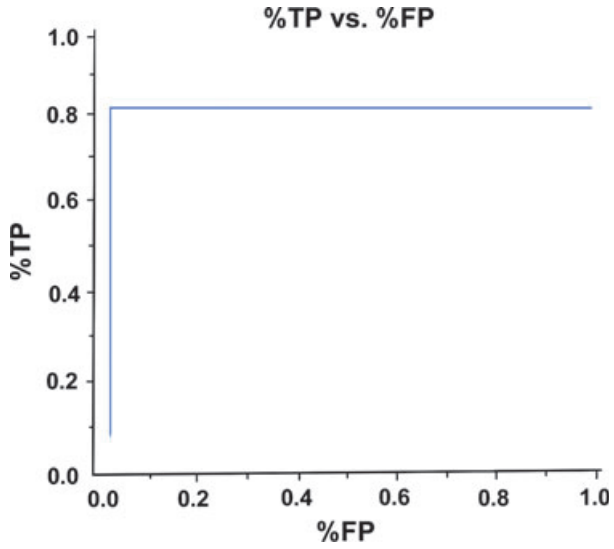

Figure 8: Cross-validation receiver operating curve (ROC) curve generated by leave-one-out method.

Table 1: Summary table for the Bayesian model

XV ROC AUC	Best split	TP/FN FP/TN	No. in Category
0.821	6.279	6/2 1/6	8

ROC, receiver operating curve.

Results of the Bayesian model indicated the 1,4-diazepane-2,5-diones ring system substituted with arylsulfonyl moiety and benzyl group substituted with halogen and alkoxy as regions mainly essential for chymase inhibition. Analysis of binding interactions between inhibitors and the active site of chymase and examination of their electronic structures also manifested that aforementioned substructures were present in most-active compounds. In contrast, most of the mid- and least-active compounds hold aminocarbonyl as part of their geometries, which was the most often substructure in Bayesian model associated with less-active inhibitors. Thus, outcome of Bayesian model not only abetted in identifying regions vital for chymase inhibition activity but also pertained as a validation technique for docking and electronic feature results.

Genetic function approximation models

To facilitate a systematic evaluation on 1,4-diazepane-2,5-diones derivatives as chymase inhibitors and to explore the more potent and selective chymase inhibitors, GFA QSAR models were built using the molecular docking parameters, DFT descriptors, and some other 2D and 3D physiochemical properties (stated previously in Section) of compounds as candidates of the descriptors. The pIC50 of the compounds was taken as the dependent variable. To produce reliable results, it typically needs five times as many compounds as independent variables. Because only 15 compounds are used in the training set for the QSAR construction and too many descriptors will make the obtained model less significant statistically, the number of descriptors tried in the subset was confined from 2 to 3. The model was optimized, and descriptors were reduced with the GFA. To determine the optimal number of explanatory terms (QSAR descriptors), it was decided to scan and evaluate all possible QSAR models resulting from 2 to 3 explanatory terms. Various models were generated and evaluated. Four models were selected for final assessment (Table 2). The statistical qualities of the models were judged by the parameters such as coefficient of determination (r^2); r^2_{adj} adjusted for the number of terms in the model; r^2_{pred} the prediction (PRESS) r^2, equivalent to q^2 from a LOO cross-validation; and Friedman LOF, which is the Friedman LOF score. To explore the prediction ability of the selected descriptors, external validation using test set method was also performed for all four models. Test set was comprised of 12 compounds. Analysis of the models was performed based on the aforementioned statistical qualities and test set upshots. Model 1 with three descriptors (Molecular_FractionalPolarSurfaceArea, Jurs_TPSA, external van der) in its equation showed best correlation (r^2 = 0.812) with r^2_{pred} value of 0.634, and its test set also exhibited high r^2 gain than test set result of other models (Figure 10A).

$$pIC_{50} = -17.155 + 25.525 * \text{Molecular\_Fractional Polar Surface Area} - 0.011149 * \text{Jurs\_TPSA} + 0.22276 * \text{External van der} \quad (1)$$

This equation indicates that Molecular_FractionalPolarSurfaceArea and external van der, which are 2D and 3D descriptors, respectively, contributed to the activity of chymase inhibitors positively, while Jurs_TPSA(3D Jurs descriptor), which calculates total polar surface area of the compound, contributed negatively to the chymase inhibition activity. We confirmed the requirements devised by Golbraikh

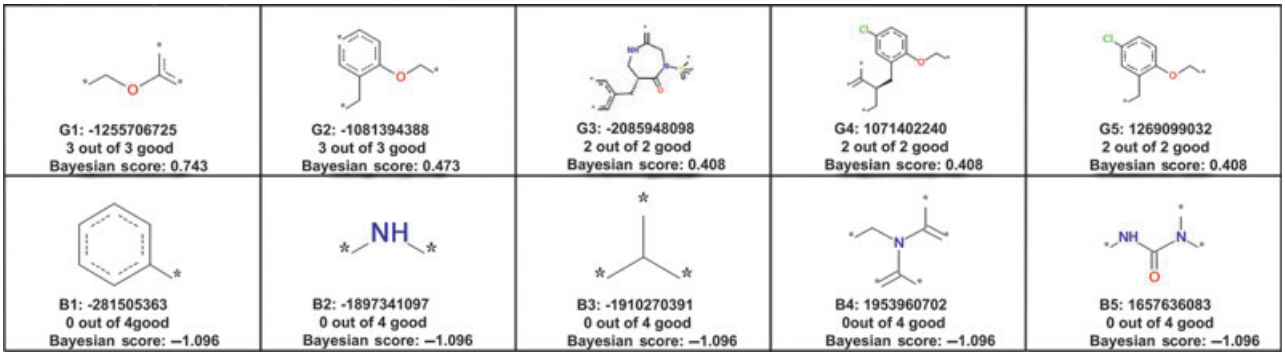

Figure 9: Top five good (G1–G5) and bad (B1–B5) molecular fingerprints identified by FCFP_6 fingerprint descriptor.

Table 2: The description of statistically significant parameters for four selected GFA models

Model	r^2	r^2_{adj}	r^2_{pred}	L.O.F	$r^2_{Testset}$
1	0.812	0.761	0.634	1.153	0.636
2	0.789	0.732	0.648	0.583	0.600
3	0.712	0.669	0.584	0.531	0.594
4	0.694	0.644	0.484	0.570	0.517

GFA, genetic function approximation.

and Trophsa for consideration of a QSAR model as highly predictive if it verifies the following conditions: (a) $q^2 > 0.5$; (b) r^2 test > 0.5 (r^2 test is the correlation coefficient for test set predictions) (41). The GFA model 1 exhibited good predictive ability by showing both q^2 and r^2 test values above 60%. However, model 1 showed relatively high score (1.153) of LOF parameter. Model 3 demonstrated equation with only two descriptors including Molecular_Fractional-PolarSurfaceArea and external van der, yet low r^2 values and diminutive predictive ability of this model bequeath it with lesser quality. Equation of model 4 was also comprised of two parameters including external van der and LUMO from docking and DFT calculations, respectively. This model exhibited lowest r^2 value (0.69), and its predictive ability dwindled to lowest among all four selected models (Table 2). However, model 2 showed good results, and the equation of the model 2 was obtained with three descriptors (Molecular_PolarSurfaceArea, E_DIST_mag, and external van der). The value of r^2 (0.78) for this model is the second highest among selected models, and LOF was also much low than that of the first model. In addition, good outcome of other statistically significant parameters like r^2_{adj}, r^2_{pred}, and r^2 of test set endowed model 2 as better model than GFA models 3 and 4, respectively. Both GFA models 1 and 2 were further validated using an external validation set consisting of 55 structurally diverse compounds with wide activity range. These chemical compounds experimentally known for the inhibition of chymase were retrieved from various literature resources (5,19,23–25,43). Genetic function approximation models 1 and 2 showed correlation of 0.716 and 0.622, respectively, for validation set, which further validated the predictive ability of these GFA models. Equation of GFA model 2 is as follows:

$$pIC_{50} = -12.142 + 0.038377 * \text{Molecular\_Polar Surface Area} - 0.00035736 * \text{E\_DIST\_mag} + 0.20973 * \text{External van der} \quad (2)$$

The number of compounds is 15, $r_2 = 0.789$, $r^2_{adj} = 0.732$, $r^2_{pred} = 0.648$, and LOF = 0.583. This model is a 2D and 3D hybrid QSAR model amalgamating three descriptors, including 2D surface area and volume descriptor (Molecular_PolarSurfaceArea), topological descriptor (V_DIST_mag), and external van der Waals (comes from the 3D docking of the ligand with chymase). The explained variance and predicted variance of eqn 1 were 73.2% and 64.8%, respectively, of the total variance of chymase inhibitory activity. Here the result of cross-validation (LOO predicted variance, q^2) is encouraging ($q^2 > 0.5$). Moreover, the result of external validation technique showing a correlation of 60% via test set validation method is also satisfactory (Figure 10B). It can be deduced from equation of GFA model 2 that Molecular_PolarSurfaceArea and docking parameter external van der contributed affirmatively to the activity of the chymase inhibitors. Positive contribution of the polar surface area of the molecule to the activity of the chymase inhibitors also validated the MEP mapping and molecular docking results that exhibited the involvement of the regions with polar atoms usually oxygen and nitrogen in the main interactions for the effective binding of most-active compounds to the key residues of the active site of chymase. External van der Waals interaction energy also contributes positively for assessing inhibitors via GOLD fitness score. So, confirmatory input of external van der Waals interaction of the compounds to the activity of the chymase inhibitors substantiated the docking output of chymase inhibitors. Kosugi *et al.* also showed that the binding affinity of adenosine deaminase inhibitors was improved by external van der Waals interaction of the compounds with the important residues of the active site. The coefficient of V_DIST_mag (Graph-Theoretical InfoContent descriptor) index has revealed that this topological descriptor has influenced negatively on the inhibitory activity of the compounds. Thus, it is deduced that models 1 and 2 have exhibited better results among all four models. Moreover, it is evident from the analysis of all four GFA models that external van der Waals interactions,

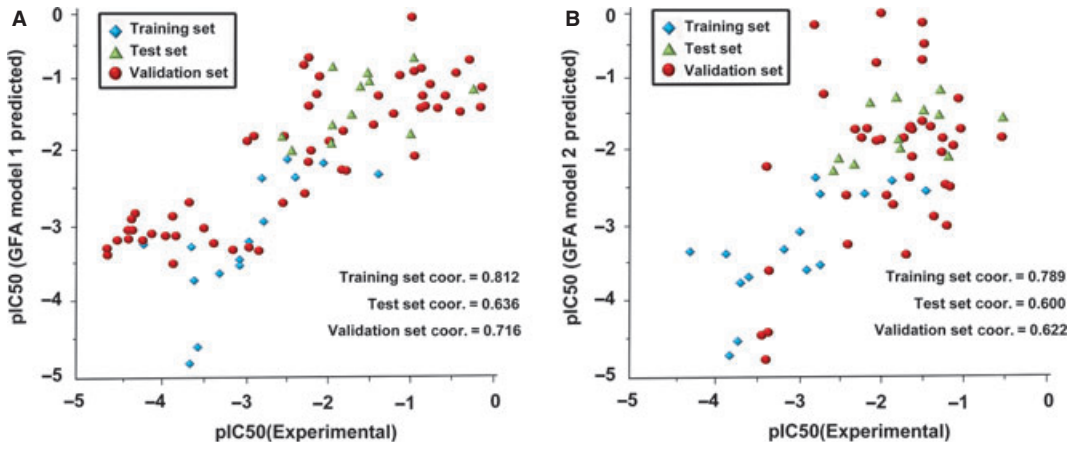

Figure 10: The plots of predicted versus experimental pIC_{50} values for training set (diamond), test set (triangle), and validation set (circle) for genetic function approximation (GFA) Model 1(A) and 2(B), respectively.

Molecular_PolarSurfaceArea, Jurs_TPSA, and E_DIST_mag are important features for chymase inhibitors. Especially, presence of Molecular_PolarSurfaceArea and external van der Waals interactions in all four models confer that these features have more significance for the activity of chymase inhibitors.

Conclusions

Using a series of theoretical methods like 2D/3D QSAR techniques, molecular docking, and DFT calculations, an investigation to develop QSAR models and to identify key factors crucial for the binding mechanism and interaction between chymase and inhibitors is performed for a novel series of chymase inhibitors. Analysis of binding conformations of ligands showed that carbonyl oxygen of 1,4-diazepane-2,5-diones ring and benzenesulfonyl chloride moiety are the most often regions that participated in important interactions with the key active site residues like Gly193, Ser195, Phe191, and Lys192. Using DFT, the detailed electronic structure description was obtained by analysis of HOMO, LUMO, and electrostatic potential distribution. Along with maps of HOMO and LUMO, molecular electrostatic profiles of the compounds were also consistent with the binding conformations of ligands generated by docking. Particularly appearance of localized negative potential regions over the carbonyl oxygen of the 7-membered ring system and oxygen atoms of benzenesulfonyl chloride group was found to be important for better activity of compounds. Moreover, different statistical methods, including Bayesian categorization, and fully cross-validated GFA were applied to construct QSAR models. The Bayesian model with LOO cross-validation ROC statistic of 0.82 recognized 1,4-diazepane-2,5-diones ring system substituted with arylsulfonyl moiety and benzyl group substituted with halogen and alkoxy as regions primarily imperious for chymase inhibition and aminocarbonyl as the segment associated with less-active inhibitors. Thus, outcome of Bayesian model not only assisted in identifying imperative regions for chymase inhibition activity but also served as a validation method for docking and electronic features results. For our data set, two GFA models (GFA model 1 r^2 = 0.812 and GFA model 2 r^2 = 0.783) performed better in terms of correlation coefficients and cross-validation analysis. A number of molecular descriptors were identified as being correlated with chymase inhibition activity. The Molecular_PolarSurfaceArea and external van der Waals features were ascertained as essential factors for the activity of chymase inhibitors. The results obtained from this study should aid in efficient design and development of novel series of 1,4-diazepane-2,5-diones derivatives as chymase inhibitors. In general, this study is used as example to illustrate how combinational use of 2D/3D QSAR modeling techniques, molecular docking, frontier molecular orbital density fields (HOMO and LUMO), and molecular electrostatic potential analysis can be useful to gain an insight into the binding mechanism between enzyme and its inhibitors.

Acknowledgments

This research was supported by Basic Science Research Program (2009-0073267), Pioneer Research Center Program (2009-0081539), and Management of Climate Change Program (2010-0029084) through the National Research Foundation of Korea (NRF) funded by the Ministry of Education, Science and Technology (MEST) of Republic of Korea. And this work was also supported by the Next-Generation BioGreen 21 Program (PJ008038) from Rural Development Administration (RDA) of Republic of Korea.

References

1. Nayana R.S., Bommisetty S.K., Singh K., Bairy S.K., Nunna S., Pramod A., Muttineni R. (2009) Structural analysis of carboline derivatives as inhibitors of MAPKAP K2 using 3D QSAR and docking studies. J Chem Inf Model;49:53–67.
2. Vainio M.J., Puranen J.S., Johnson M.S. (2009) ShaEP: molecular overlay based on shape and electrostatic potential. J Chem Inf Model;49:492–502.
3. Nam K., Gao J.L., York D.M. (2008) Electrostatic interactions in the hairpin ribozyme account for the majority of the rate acceleration without chemical participation by nucleobases. RNA;14:1501–1507.
4. Daga P.R., Doerksen R.J. (2008) Stereoelectronic properties of spiroquinazolinones in differential PDE7 inhibitory activity. J Comput Chem;29:1945–1954.
5. Waller C.L., Marshall G.R. (1993) Three-dimensional quantitative structure-activity relationship of angiotesin-converting enzyme and thermolysin inhibitors. II. A comparison of CoMFA models incorporating molecular orbital fields and desolvation free energies based on active-analog and complementary-receptor-field alignment rules. J Med Chem;36:2390–2403.
6. Navajasra C., POSO A., Tuppurainenb T., Gynthe J. (1996) Comparative molecular field analysis (CoMFA) of NIX compounds using different semi-empirical methods: LUMO field and its correlation with mutagenic activity. Quant Struct Act Relat;5:189–193.
7. Ruiz J., Pe′rez C., Pouplana R. (2003) QSAR study of dual cyclooxygenase and 5-lipoxygenase inhibitors 2, 6-di-tert-butylphenol derivatives. Bioorg Med Chem;11:4207–4216.
8. Díaz L., Bujons J., Delgado A., Guti H., Åqvist J. (2011) Computational prediction of structure-activity relationships for the binding of aminocyclitols to β-glucocerebrosidase. J Chem Inf Model;51:601–611.
9. Caughey G.H., Raymond W.W., Wolters P.J. (2000) Angiotensin II generation by mast cell α- and β-chymases. Biochim Biophys Acta;1480:245–257.
10. Amano N., Takai S., Jin D., Ueda K., Miyazaki M. (2009) Possible roles of mast cell-derived chymase for skin rejuvenation. Lasers Med Sci;24:223–229.
11. Takai S., Miyazaki M. (2005) Inhibition of transforming growth factor- activation is a novel effect of chymase inactivation. Lett Drug Des Discov;2:19–22.
12. Omoto Y., Tokime K., Yamanaka K., Habe K., Morioka T., Kurokawa I., Tsutsui H., Yamanishi K., Nakanishi K., Mizutani H. (2006) Human mast cell chymase cleaves Pro-IL-18 and generates a novel and biologically active IL-18 fragment. J Immunol;177:8315–8319.
13. Huang X.R., Chen W.Y., Truong L.D., Lan H.Y. (2003) Chymase is upregulated in diabetic nephropathy: implications for an alternative pathway of angiotensin II-mediated diabetic renal and vascular disease. J Am Soc Nephrol;14:1738–1747.

14. Garavilla L.D., Greco M.N., Sukumar N., Chen Z., Pineda A.O., Mathews F.S., Cera E.D. *et al.* (2005) A novel, potent dual inhibitor of the leukocyte proteases cathepsin G and chymase. J Biol Chem;280:18001–18007.
15. Powers J.C., Tanaka T., Harper J.W., Minematsu Y., Baker L., Lincoln D., Crumley K.V. (1985) Mammalian chymotrypsin-like enzymes. Comparative reactivities of rat mast cell proteases, human and dog skin chymases, and human cathepsin G with peptide 4-nitroanilide substrates and with peptide chloromethyl ketone and sulfonyl fluoride inhibitors. Biochemistry;24:2048–2058.
16. Burzycki T.A., Hoover K.W., Thomsen D.L., Sneddon S.F., Rauch A.L., Hoover D.J. (1993) IBC conference on developmental therapy for hypertension: beyond ACE inhibitors and calcium antagonists. Philadelphia.
17. Bastos M., Maeji N.J., Abeles R.H. (1995) Inhibitors of human heart chymase based on a peptide library. Proc Natl Acad Sci USA;92:6738–6742.
18. Greco M.N., Hawkins M.J., Powell E.T., Almond H.R., Garavilla L., Hall J., Minor L.K., Wang Y., Corcoran T.W., Cera E.D., Cantwell A.M., Savvides S.N., Damiano B.P., Maryanoff B.E. (2007) Discovery of potent, selective, orally active, nonpeptide inhibitors of human mast cell chymase. J Med Chem;50:1727–1730.
19. Iijima K., Katada J., Yasuda E., Uno I., Hayashi Y. (1999) N-[2,2-Dimethyl-3-(N-(4-Cyanobenzoyl)Amino)Nonanoyl]-L-Phenylalanine ethyl ester as a stable ester-type inhibitor of chymotrypsin-like serine proteases: structural requirements for potent inhibition of α-chymotrypsin. J Med Chem;42:312–323.
20. Aoyama Y., Uenaka M., Kii M., Tanaka M., Konoike T., Hayasaki-Kajiwara Y., Naya N., Nakajima M. (2001) Design, synthesis and pharmacological evaluation of 3-benzylazetidine-2-one-based human chymase inhibitors. Bioorg Med Chem;9:3065–3075.
21. Aoyama Y., Uenaka M., Konoike T., Hayasaki-Kajiwara Y., Naya N., Nakajima M. (2001) Inhibition of serine proteases: activity of 1, 3-Diazetidine-2, 4-diones. Bioorg Med Chem Lett;11:1691–1694.
22. Aoyama Y., Konoike T., Kanda A., Naya N., Nakajima M. (2001) Total synthesis of human chymase inhibitor methyllinderone and structure–activity relationships of its derivatives. Bioorg Med Chem Lett;11:1695–1697.
23. Hayashi Y., Iijima K., Katada J., Kiso Y. (2000) Structure-activity relationship studies of chloromethyl ketone derivatives for selective human chymase inhibitors. Bioorg Med Chem Lett;10:199–201.
24. Aoyama Y., Uenaka M., Konoike T., Iso Y., Nishitani Y., Kanda A., Naya N., Nakajima M. (2000) Synthesis and structure-activity relationships of a new class of 1-oxacephem-based human chymase inhibitors. Bioorg Med Chem Lett;10:2397–2401.
25. Niwata S., Fukami H., Sumida M., Ito A., Kakutani S., Saitoh M., Suzuki K. *et al.* (1997) Substituted 3-(Phenylsulfonyl)-1-phenylimidazolidine-2,4-dione derivatives as novel nonpeptide inhibitors of human heart chymase. J Med Chem;40:2156–2163.
26. Iijima K., Katada J., Hayashi Y. (1999) Symmetrical anhydride-type serine protease inhibitors:structure-activity relationship studies of human chymase inhibitors. Bioorg Med Chem Lett;9:413–418.
27. Tanaka T., Muto T., Maruoka H., Imajo S., Fukami H., Tomimori Y., Fukudaa Y., Nakatsuka T. (2007) Identification of 6-substituted 4-arylsulfonyl-1,4-diazepane- 2,5-diones as a novel scaffold for human chymase inhibitors. Bioorg Med Chem Lett;17:3431–3434.
28. Maruoka H., Muto T., Tanaka T., Imajo S., Tomimori Y., Fukudaa Y., Nakatsuka T. (2007) Development of 6-benzyl substituted 4-aminocarbonyl-1,4- diazepane-2,5-diones as orally active human chymase inhibitors. Bioorg Med Chem Lett;17:3435–3439.
29. Wawer M., Bajorath J. (2010) Similarity-potency trees: a method to search for SAR information in compound data sets and derive SAR rules. J Chem Inf Model;50:1395–1409.
30. Thangapandian S., John S., Sakkiah S., Lee K.L. (2011) Molecular docking and pharmacophore filtering in the discovery of dual-inhibitors for human leukotriene A4 hydrolase and leukotriene C4 synthase. J Chem Inf Model;51:33–44.
31. Lie M.A., Thomsen R., Pedersen C.N.S., Schiøtt B., Christensen M.H. (2011) Molecular docking with ligand attached water molecules. J Chem Inf Model;5:909–917.
32. Liu T.Q., Lin Y.M., Wen X., Jorissen R.N., Gilson M.K. (2007) BindingDB: a web-accessible database of experimentally determined protein-ligand binding affinities. Nucleic Acids Res;35:D198–D201.
33. Hartshorn M.J., Verdonk M.L., Chessari G., Brewerton S.C., Mooij W.T.M., Mortenson P.N., Murray C.W. (2007) Diverse, high-quality test set for the validation of protein-ligand docking performance. J Med Chem;50:726–741.
34. Cole J.C., Nissink J.W.M., Taylor R. (2005) Protein-ligand docking and virtual screening with GOLD. In: Shoichet B., Alvarez J., editors. Virtual Screening in Drug Discovery. Boca Raton, FL, USA: Taylor & Francis CRC Press.
35. Yaozong Li., Jie S., Xianqiang S., Weihua L., Guixia L., Yun T. (2010) Accuracy assessment of protein-based docking programs against RNA targets. J Chem Inf Model;50:1134–1146.
36. Lee C., Yang W., Parr R.G. (1988) Development of the colle-salvetti correlation-energy formula into a functional of the electron density. Phys Rev;37:785–789.
37. Kenny P.W. (2009) Hydrogen bonding, electrostatic potential, and molecular design. J Chem Inf Model;49:1234–1244.
38. Dehez F., Pebay-Peyroula E., Chipot C. (2008) Binding of ADP in the mitochondrial ADP/ATP carrier is driven by an electrostatic funnel. J Am Chem Soc;130:12725–12733.
39. Rogers D., Hopfinger A.J. (1994) Application of genetic function approximation to quantitative structure-activity relationships and quantitative structure-property relationships. J Chem Inf Comput Sci;34:854–866.
40. Richon A.B., Young S.S. (1997) An Introduction to QSAR Methodology. Saluda, NC: Network Science Corporation.
41. Golbraikh A., Tropsha A. (2002) Beware of q2!. J Mol Graph Model;20:269–276.
42. Arooj M., Thangapandian S., John S., Hwang S., Park J.K., Lee K.W. (2011) 3D QSAR pharmacophore modeling, in silico screening, and density functional theory (DFT) approaches for identification of human chymase inhibitors. Int J Mol Sci;12:9236–9264.
43. Greco M., Hawkins M., Garavilla L.D., Powell E., Maryanoff B.E. (2008) Patent US20080096844 A1.

Supporting Information

Additional Supporting Information may be found in the online version of this article:

Figure S1. Overall 3D structure of human chymase and the zoomed view that clearly shows the important catalytic residues.

Figure S2. Molecular docking validation results: overlay of the docked poses (gray) of inhibitors with their crystal structure conformation (green for 3N7O, pink for 3SON).